Nano Energy 65 (2019) 104001

Contents lists available at ScienceDirect

Nano Energy

journal homepage: www.elsevier.com/locate/nanoen

Full paper

$WS_2/CsPbBr_3$ van der Waals heterostructure planar photodetectors with ultrahigh on/off ratio and piezo-phototronic effect-induced strain-gated characteristics

Qian Xu[a,b], Zheng Yang[a,b], Dengfeng Peng[d], Jianguo Xi[a], Pei Lin[f], Yang Cheng[e], Kaihui Liu[e], Caofeng Pan[a,b,c,d,*]

[a] CAS Center for Excellence in Nanoscience, Beijing Key Laboratory of Micro-nano Energy and Sensor, Beijing Institute of Nanoenergy and Nanosystems, Chinese Academy of Sciences, Beijing, 100083, PR China
[b] School of Nanoscience and Technology, University of Chinese Academy of Sciences, Beijing, 100049, PR China
[c] Center on Nanoenergy Research, School of Physical Science and Technology, Guangxi University, Nanning, Guangxi, 530004, PR China
[d] College of Optoelectronic Engineering, Shenzhen University, Shenzhen, 518060, PR China
[e] State Key Laboratory for Mesoscopic Physics, Collaborative Innovation Centre of Quantum Matter, School of Physics, Peking University, Beijing, 100871, PR China
[f] Department of Physics and Engineering, Zhengzhou University, Zhengzhou, Henan, 450052, PR China

ARTICLE INFO

Keywords:
WS_2
$CsPbBr_3$
Photodetectors
Piezo-phototronic effect
Van der Waals heterostructures

ABSTRACT

High-performance, low-power and multifunction-integrated devices are crucial in emerging technologies. Herein, we demonstrate $WS_2/CsPbBr_3$ van der Waals heterostructure (vdWH) planar photodetectors combining the high mobility of mechanically exfoliated 2D WS_2 nanoflakes with the remarkable optoelectronic properties of 1D single-crystalline $CsPbBr_3$ nanowires and the strain-gated and strain-sensing characteristics induced by the piezo-phototronic effect. Owing to the effective charge carrier transfer and channel depletion originating from the appropriate energy band alignment, collaborative improvement of the photocurrent and dark current is realized, thus, an ultrahigh on/off ratio of $10^{9.83}$ is achieved. The highest responsivity and detectivity at $V_d = 2$ V are 57.2 A W^{-1} and 1.36×10^{14} Jones, respectively. Even with a lower V_d of 0.5 V, decent performance is still obtained. Furthermore, the interfacial carrier transfer can be manipulated through the piezo-phototronic effect induced by $CsPbBr_3$ monocrystal nanowires. Thus, when constructed on a flexible PEN substrate, the $WS_2/CsPbBr_3$ vdWH planar photodetector presents strain-gated photocurrent and responsivity, modulated by a factor of 11.3 with strain application, and a strain-sensing function is simultaneously realized due to the linear dependence of the photocurrent on strain. This unprecedented device design opens up a new avenue toward not only high-performance and low-power but also multifunction-integrated devices realized by the direct effect of mechanical inputs on charge carriers.

1. Introduction

As a kind of novel material with great potential, two-dimensional (2D) materials are widely studied for electronic and optoelectronic applications owing to their ultrathin thickness, tunable bandgaps and high mobility [1–5]. The interlayer van der Waals (vdW) force and atomically flat interface help 2D materials escape the restrictions arising from lattice matching in heterostructure construction [3,6–8]. Due to the high possibility of combining 2D materials with materials of various dimensions, state-of-the-art optoelectronic heterostructures can be manufactured. Inspired by these efforts, halide perovskites with remarkable optoelectronic properties [9–11] have been used to assemble heterostructures with 2D materials. Effective and ultrafast charge carrier transfer between perovskites and 2D materials has been widely demonstrated and has been shown to dramatically improve the performance of planar photodetectors [4,12–16]. However, without modulation of gate voltage, the dark currents of these planar 2D-material/perovskite photodetectors are so great that the on/off ratio is low and the standby power is large, which greatly restricts the application of 2D-material/perovskite photodetectors [13,14,17]. Owing to the depletion in WS_2, chemical vapor deposition (CVD)-synthesized monolayer $WS_2/CH_3NH_3PbI_3$ thin film heterostructure photodetectors

* Corresponding author. CAS Center for Excellence in Nanoscience, Beijing Key Laboratory of Micro-nano Energy and Sensor, Beijing Institute of Nanoenergy and Nanosystems, Chinese Academy of Sciences, Beijing, 100083, PR China.
E-mail address: cfpan@binn.cas.cn (C. Pan).

https://doi.org/10.1016/j.nanoen.2019.104001
Received 6 June 2019; Received in revised form 24 July 2019; Accepted 7 August 2019
Available online 10 August 2019

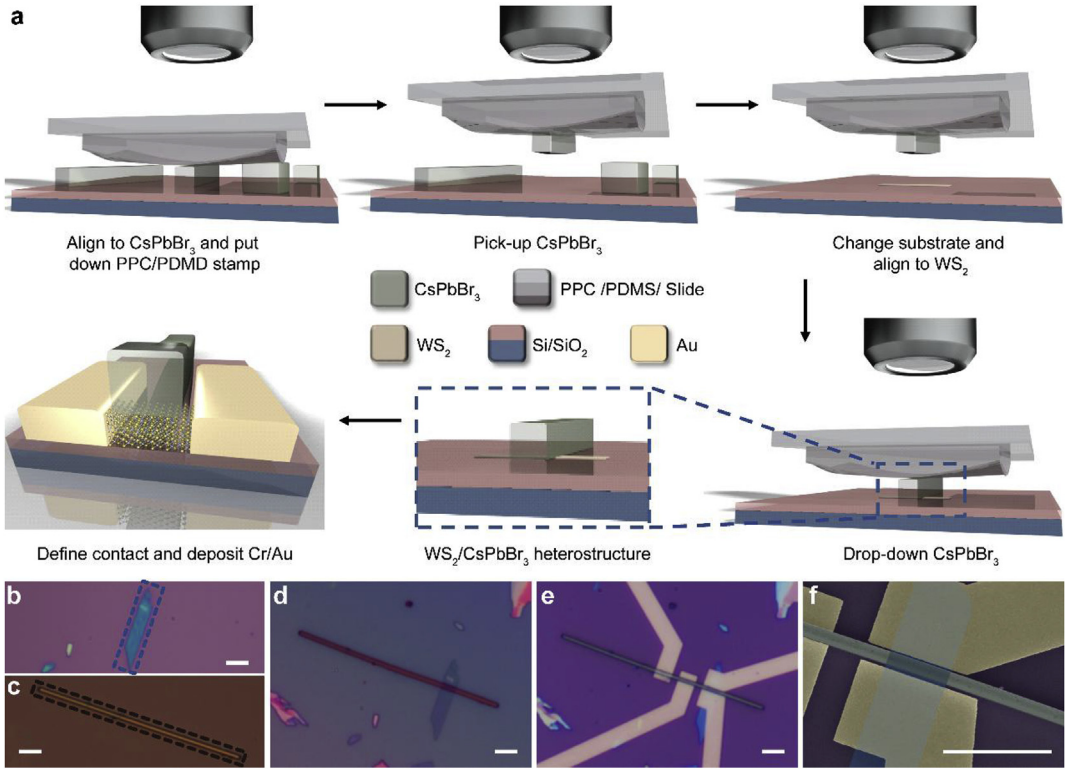

Fig. 1. Assembly processes and device structure of $WS_2/CsPbBr_3$ vdWHs. (a) Schematic illustration of device assembly. (b) and (c) Optical micrographs of the chosen 2D WS_2 flake and 1D $CsPbBr_3$ nanowire for building a vdWH, respectively. (d) Optical micrographs of the assembled $WS_2/CsPbBr_3$ vdWH coated by PMMA. (e) and (f) Optical micrographs and false-color SEM image of the $WS_2/CsPbBr_3$ vdWH planar photodetector, respectively. Notably, the metal contacts across the $CsPbBr_3$ nanowire are useless in this work. All the scale bars in (b) ~ (f) are 5 μm.

[15] displayed a good performance with a 10^5 on/off ratio and a 10^{12} Jones detectivity, but the weak mobility limited the performance and the high operating voltage hampered the reduction of energy consumption.

All of the previous reports on 2D-material/perovskite photodetectors utilize 2D material synthesized by CVD or solution process. While mechanical cleavage enables 2D flakes with higher purity and cleanliness to be more easily obtained [1]. The better crystal quality, fewer defects and higher mobility of mechanically exfoliated 2D flakes can endow photodetectors with much higher performance and lower energy dissipation. Moreover, all of these reported heterostructures overwhelmingly employ organic–inorganic hybrid halide perovskites. These perovskites are not stable for many solvents which imposes severe limitations on device construction. Perovskites with disordered orientations, such as polycrystal [12,14,18], quantum dot (QD) [17] and multiple monocrystal [19], were usually used, thus it is a challenge to realize piezotronic or piezo-phototronic effect through the piezoelectric property of halide perovskites. All-inorganic halide perovskite monocrystals, such as $CsPbBr_3$, with much better stability, no grain boundaries, a lower trap density and longer carrier diffusion exhibit great potential for constructing high-performance devices. Very recently, the piezoelectric property of $CsPbBr_3$ [20] has been reported, however the piezotronic or piezo-phototronic effect induced by $CsPbBr_3$ has not been reported. Piezotronic and piezo-phototronic effects endow traditional devices with not only better performance but also multifunction integration, which is crucial for wearable electronics, human-machine interfaces, the Internet of things, etc [21]. Considering the excellent properties of both mechanically exfoliated 2D flakes and all-inorganic halide perovskite monocrystals, a high-performance, low-power and multifunction-integrated vdWH photodetector can be potentially realized by employing these two kinds of building blocks.

In this study, mechanically exfoliated 2D WS_2 nanoflakes and single-crystalline 1D $CsPbBr_3$ nanowires are employed to construct $WS_2/CsPbBr_3$ vdWH planar photodetectors for the first time. Attributed to both effective charge carrier transfer and channel depletion, photocurrent enhancement and dark current suppression are simultaneously observed. The assembled devices exhibit an on/off ratio, a responsivity, and a detectivity of up to $10^{9.83}$, 57.2 A W^{-1}, and 1.36×10^{14} Jones, respectively. Compared with previous reports, the high crystal quality of mechanically exfoliated 2D WS_2 gives rise to a significant reduction in V_d. The enhanced photocurrent, ultralow dark current, and significantly reduced V_d endow the $WS_2/CsPbBr_3$ vdWH photodetector with low-power and high-performance characteristics. Furthermore, the vdWH photodetector are fabricated on flexible PEN substrate. Through the piezo-phototronic effect, carrier transfer at the interface is modulated. In addition to the performance modulation of the $WS_2/CsPbBr_3$ vdWH photodetector, the response to an applied strain is also demonstrated. Thus, high-performance, low-power and multifunction-integrated characteristics are achieved through $WS_2/CsPbBr_3$ vdWHs.

2. Experimental section

2.1. $CsPbBr_3$ nanowire synthesis

The method has been previously reported [11,20,22]. To prepare the precursor solution, 4 M CsBr and $PbBr_2$ are simultaneously dissolved in DMSO at 50 °C, and then, MeCN is added dropwise into the solution until the solution reaches saturation through vigorously stirring for 24 h at 50 °C. After filtration, the solution is dropped onto a hydrophilic Si/SiO_2 substrate using a pipette, and a hydrophobic PDMS template is placed onto the solution. The Si/SiO_2 substrate and PDMS are pressed together. After incubation at 40 °C for 24 h, $CsPbBr_3$ nanowires and microwires can be grown on the Si/SiO_2 substrates. In this work, only nanowires with diameters varying from 400 nm–1 μm are

used.

2.2. Fabrication process of $WS_2/CsPbBr_3$ vdWH planar photodetectors

The entire fabrication process of vdWHs is illustrated in Fig. 1a. To build 2D-WS_2/1D-$CsPbBr_3$ vdWHs on a substrate (Si/SiO_2 or PEN), few-layer WS_2 flakes (Fig. 1b) are first exfoliated onto the target substrate. Then, a $CsPbBr_3$ nanowire (Fig. 1c) with diameter of 400 nm–1 μm are precisely transferred onto WS_2 through a picking-up and dropping process using the PPC/PDMS stamp. As illustrated in Fig. 1a, a PPC/PDMS stamp adhered on a slide is aligned and contact with the target $CsPbBr_3$ nanowire. After heating to 60 °C and then cooling to 40 °C, the $CsPbBr_3$ nanowire is picked-up by the PPC/PDMS stamp. Next, the selected 2D WS_2 flake on the target substrate is placed under a microscope and aligned with the $CsPbBr_3$ nanowire. Finally, the $CsPbBr_3$ nanowire is precisely dropped onto the WS_2 flake (Fig. 1d).

Before use as a substrate, PEN is cut into circular pieces 2 cm in diameter, and a 100 nm SiO_2 layer is deposited on it by magnetron sputtering (Kurt J. Lesker PVD75). SiO_2 acts as an adhesion layer because the $CsPbBr_3$ nanowire cannot be directly attached to the PEN substrate.

To fabricate $WS_2/CsPbBr_3$ vdWH planar photodetectors, contacts are defined by an electron beam lithography (EBL) process (FEI Helios NanoLab 600i with a Raith SEM-pattern generator), followed by deposition and liftoff of Cr/Au (10/40 nm).

2.3. Characterization and measurement of $WS_2/CsPbBr_3$ vdWH planar photodetectors

The PL, PL mapping and corresponding decay curve are obtained by steady-state/transient fluorescence spectrometry (FLS980). The crystalline phase of the $CsPbBr_3$ nanowires is determined by XRD (PANalytical X'Pert3). HR-TEM and SAED of $CsPbBr_3$ nanowires are conducted (FEI Tecnai G2 F20 S-TWIN TMP) at an accelerating voltage of 80 kV. I-V curves of the photodetectors are measured by a Keithley 4200-SCS. A Stanford DS345 and an SR570 are employed for I-T measurements. The incident power of the 450 nm laser is modulated by an attenuator. When the photodetectors are measured under strain, a manual stage is used as shown in Fig. S5. All electrical measurements are conducted at room temperature.

2.4. Fabrication and measurement of WS_2 photodetectors

To compare photodetector performance of $WS_2/CsPbBr_3$ vdWH with pristine WS_2, pristine WS_2 photodetectors are fabricated. The fabrication details of WS_2 devices are as same as those of $WS_2/CsPbBr_3$ devices, except there is no need for constructing vdWHs. And the measurement method is also totally same with that of $WS_2/CsPbBr_3$ devices.

3. Results and discussion

An optical image of the as-fabricated device is shown in Fig. 1e. Notably, the metal contacts across the $CsPbBr_3$ nanowire are useless in this work. The SEM image (Fig. 1f) clearly shows that the contacts on the WS_2 channel do not touch the $CsPbBr_3$ nanowire, confirming that the conducting channel is only WS_2. Compared with the dual channel consisting of both a 2D material and a perovskite that has usually been used in previous reports [12–15,18], the single-channel structure in this work is used for better dark current suppression, as shown below.

To investigate the charge carrier transfer between $CsPbBr_3$ nanowires and WS_2 nanoflakes, the photoluminescence (PL) of the $WS_2/CsPbBr_3$ vdWH is measured. Fig. 2a shows that the $CsPbBr_3$ nanowire possesses a PL peak at approximately 525 nm under a 410 nm excitation laser, which is in agreement with the results in previous reports [23,24]. The PL intensity of the $WS_2/CsPbBr_3$ vdWH (point A in the inset of Fig. 2a) is smaller than that of pristine $CsPbBr_3$ (point B). The corresponding PL mapping is presented in Fig. 2b, which is measured over the entire area shown in the inset of Fig. 2a. The PL mapping is divided in half by a dashed line, and the left part (vdWH area) displays a much lower PL density than the right part (pristine $CsPbBr_3$ area). To further reveal charge carrier transfer at the interface, time-resolved photoluminescence (TRPL) measurement at points A and B are taken. As shown in Fig. 2c, the TRPL decay curves of the $WS_2/CsPbBr_3$ vdWH and pristine $CsPbBr_3$ nanowire are well fitted by a single-exponential function [4]. According to the fitting results, the lifetimes of $WS_2/CsPbBr_3$ and $CsPbBr_3$ exciton radiative recombination are 0.84 ns and 1.04 ns, respectively. The PL quenching and the shorter exciton recombination lifetime of the $WS_2/CsPbBr_3$ vdWH are the results of charge carrier transfer from $CsPbBr_3$ nanowires to WS_2 nanoflakes [4,15]. The band profile of the $WS_2/CsPbBr_3$ vdWH is illustrated in Fig. 2d, according to previous reports [1,4,15,16,25]. Because of the appropriate band alignment, under the excitation light, some of the light-induced carriers in $CsPbBr_3$ are transferred to WS_2. Due to the different barriers for electrons and holes, electrons are transferred more easily, and some excitons in $CsPbBr_3$ are dissociated. As a result, the radiative recombination is weakened. Meantime, the PL intensity and PL lifetime are reduced. Notably, considering the small thickness and high carrier density of 2D WS_2 flakes compared to $CsPbBr_3$ nanowires, the entire WS_2 area in good contact with $CsPbBr_3$ should be depleted, and no flat band part is observed in the vdWH area of WS_2. Thus, the flat band part of WS_2 shown in Fig. 2d is included here only for convenience in depicting the excited and transferred charge carriers within WS_2.

Raman spectra are important for revealing the structure of 2D materials. As depicted in Fig. 2e, under a 633 nm excitation laser, the main WS_2 Raman peaks of 2LA(M) at 351.27 cm^{-1} and $A_{1g}(\Gamma)$ at 419.73 cm^{-1} are obtained in the pristine WS_2 area [26] (point C in the inset of Fig. 2a), while no Raman peak is observed for pristine $CsPbBr_3$ (point B) except for the peak at 520 cm^{-1} from the Si/SiO_2 substrate. For the $WS_2/CsPbBr_3$ vdWH (point A), the Raman spectrum is still dominated by WS_2 Raman peaks. As shown in Fig. 2f, which is a magnification of the framed area in Fig. 2e, the 2LA(M) peak at 351.27 cm^{-1} for pristine WS_2 is shifted slightly to 349.55 cm^{-1} for the $WS_2/CsPbBr_3$ vdWH, and the redshift of the 2LA(M) peak is consistent with a previous report [15]. This result indicates that the WS_2 structure is not subjected to damage during the heterostructure fabrication process.

In addition to the highly efficient charge carrier transfer, another merit of the $WS_2/CsPbBr_3$ vdWHs is the depletion of the WS_2 channel. For the pristine WS_2 channel without $CsPbBr_3$, as depicted in Fig. 2g and f, no suppression of the dark current occurs. For the $WS_2/CsPbBr_3$ vdWH planar photodetector illustrated in Fig. 2i and j, the depletion within the WS_2 channel will significantly suppress the dark current.

Fig. 3a displays I-V curves of the pristine WS_2 and $WS_2/CsPbBr_3$ vdWH photodetectors. The channel length and width of the measured WS_2 photodetector are ~1 μm and ~4.5 μm, respectively, while the channel length and width of the measured $WS_2/CsPbBr_3$ photodetector are ~1.2 μm and ~4.1 μm, respectively. The effective incident light intensity is defined as $P_{eff} = P_{in} \times (A_{device}/A_{laser})$, where P_{in} is the incident light intensity and A_{device} is the active area, equal to the product of the channel length and width. Under the same incident 450 nm laser, the P_{eff} values of the WS_2 and $WS_2/CsPbBr_3$ devices are 1.59 and 1.72 μW, respectively, which are very similar to each other. Fig. 3a shows that the dark current and photocurrent of the $WS_2/CsPbBr_3$ photodetector are suppressed and enhanced, respectively; thus, the on/off ratio is remarkably increased. Detailed statistics of the photocurrent density (J_{ph}) and on/off ratio are exhibited in Fig. 3b and c, respectively. Data from six WS_2 photodetectors and nine $WS_2/CsPbBr_3$ photodetectors are collected to obtain the statistics. J_{ph} is calculated by $J_{ph} = I_{ph}/W_{channel}$, where I_{ph} is the photocurrent ($I_{ph} = I_{light} - I_{dark}$) and $W_{channel}$ is the WS_2 channel width. A mean J_{ph} of 2.20 μA $μm^{-1}$ is obtained for the WS_2 photodetectors, and that obtained for the WS_2/

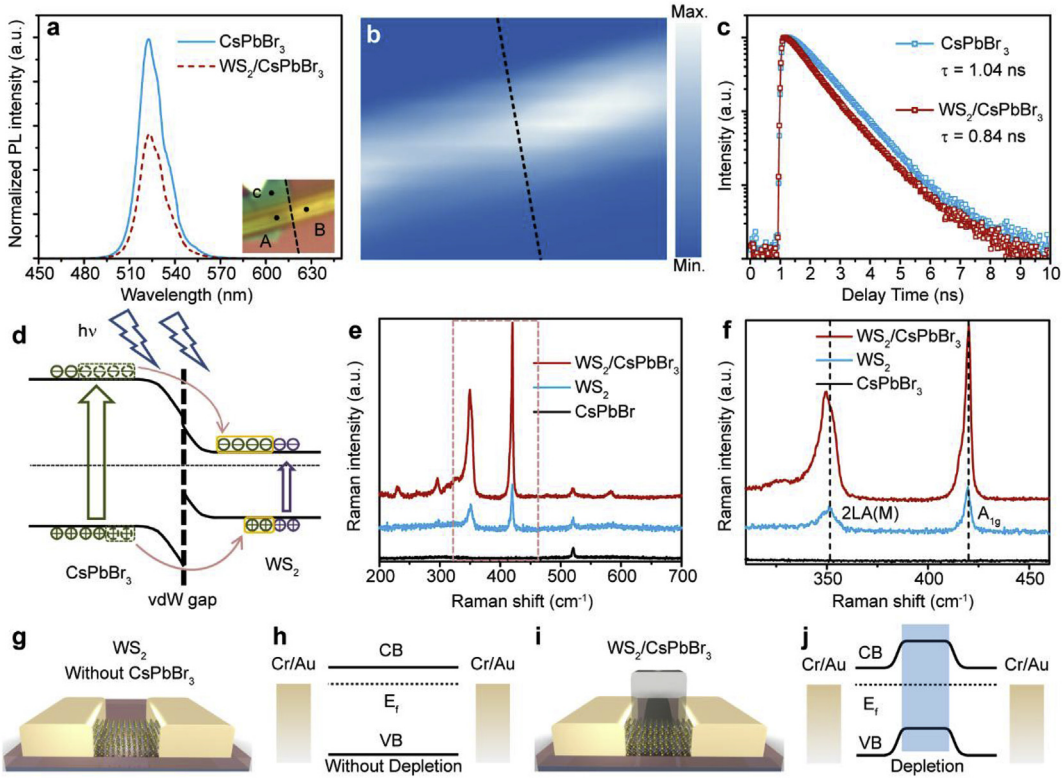

Fig. 2. Spectral patterns and band structure of a WS_2 channel section. (a) PL spectra of $CsPbBr_3$ and the $WS_2/CsPbBr_3$ vdWH, in which the inset shows the measurement points. Point A, B and C response $WS_2/CsPbBr_3$ vdWH, pristine $CsPbBr_3$ and pristine WS_2, respectively. (b) PL mapping of the $WS_2/CsPbBr_3$ vdWH. The dashed line corresponds to that shown in the inset of (a). (c) TRPL spectra of $CsPbBr_3$ and the $WS_2/CsPbBr_3$ vdWH. (d) Band structure of $WS_2/CsPbBr_3$ vdWHs, illustrating that charge carriers transfer from $CsPbBr_3$ to WS_2. (e) Raman spectra of $WS_2/CsPbBr_3$, WS_2, and $CsPbBr_3$ acquired under a 633 nm laser. (f) Magnification of the area indicated by the rectangular frame in (e). (g) and (h) Schematic illustration and band structure of the WS_2 channel section for pristine WS_2 photodetectors, respectively. (i) and (j) Schematic illustration and band structure of the WS_2 channel section for $WS_2/CsPbBr_3$ vdWH photodetectors, respectively. Notably, the entire WS_2 area in good contact with $CsPbBr_3$ should be depleted; thus, the flat band part of WS_2 in Fig. 2d is included here only for convenience in depicting the excited and transferred charge carriers within WS_2.

$CsPbBr_3$ photodetectors is nearly double this value at 4.37 μA μm^{-1}. The experimentally obtained J_{ph} values are clearly shown by the points with dashed lines in Fig. 3d, and the distribution of J_{ph} values is also presented. The overall J_{ph} of the $WS_2/CsPbBr_3$ photodetectors is almost twice that of the WS_2 photodetectors, and 66.7% of the $WS_2/CsPbBr_3$ photodetectors exceed the best J_{ph} of the WS_2 photodetectors. The noticeable increase in J_{ph} can be attributed to the efficient photon-generated carrier transfer [2,12,17] from $CsPbBr_3$ to the WS_2 channel. Moreover, both the pristine WS_2 and $WS_2/CsPbBr_3$ vdWH photodetector devices present much higher J_{ph} and much lower operating voltage than those in a previous report [15] that utilize CVD-WS_2 as channel. This result indicates that the high crystal quality of mechanically exfoliated WS_2 is well preserved in our devices. With increasing photocurrent, the dark current is suppressed through depletion of the channel (Fig. 2j). Owing to the simultaneous increase in the photocurrent and decrease in the dark current, the on/off ratios for $WS_2/CsPbBr_3$ photodetectors are dramatically increased, as shown in Fig. 3c. The mean on/off ratio of the WS_2 photodetectors is $10^{4.29}$, while that of the $WS_2/CsPbBr_3$ photodetector is as high as $10^{8.52}$. That is, an increase of more than 4 orders of magnitude is achieved. The experimentally obtained on/off ratios are presented in Fig. 3e, further showing that all $WS_2/CsPbBr_3$ photodetectors achieve higher on/off ratios than WS_2. These results preliminarily reveal the high performance of $WS_2/CsPbBr_3$ vdWH planar photodetectors.

To explicitly reveal the performance of the $WS_2/CsPbBr_3$ photodetector, I-V curves obtained under different incident light intensities are presented in Fig. 3f. Fig. 3g shows the corresponding light intensity dependence of I_{ph} at V_d = 2 V. A responsivity (R = defined as I_{ph}/P_{eff}) of as high as 57.2 A W^{-1} is observed for the $WS_2/CsPbBr_3$ photodetector in Fig. 3h, while the highest responsivity of the WS_2 device is 16.7 A W^{-1} (Fig. S2a). The responsivity presents a decrease with increasing light power. The *EQE* is calculated by $EQE = hcI_{ph}/e\lambda P_{eff}$, in which h is the Planck constant, c is the speed of light, e is the absolute value of electronic charge, and λ is the wavelength of the incident laser [27]. The highest *EQEs* of the $WS_2/CsPbBr_3$ (Fig. 3h) and WS_2 (Fig. S2c) photodetectors are 157.9 and 46.0, respectively. Fig. 3i and Fig. S2d illustrate the maximum on/off ratio and detectivity of the $WS_2/CsPbBr_3$ and WS_2 photodetectors, respectively. The maximum on/off ratio of $WS_2/CsPbBr_3$ ($10^{9.83}$) is significantly larger than that of the WS_2 device ($10^{4.76}$). The detectivity (D^*) is defined as $D^* = R/(A_{device}/2eI_{dark})^{1/2}$, and D^* values of up to 1.36×10^{14} and 1.73×10^{11} Jones, respectively, are obtained for the $WS_2/CsPbBr_3$ and WS_2 photodetectors. All the results demonstrate that the performance of the $WS_2/CsPbBr_3$ vdWH photodetector is remarkably improved by interfacial carrier transfer and depletion of the conducting channel. To present the device performance at a lower operating voltage, the corresponding I_{ph}, R and D^* of the $WS_2/CsPbBr_3$ photodetector at V_d = 0.5 V are shown in Fig. S3. According to Fig. S3, the maximum R and D^* can reach 7.3 A W^{-1} and 2.4×10^{13} Jones, with P_{eff} = 41.56 nW. Thus, the $WS_2/CsPbBr_3$ photodetector can still show good performance at a lower operating voltage of 0.5 V, which clearly reduces the device energy consumption. The time-dependent photocurrent response of the $WS_2/CsPbBr_3$ photodetector is revealed in Fig. 3j. Rise and decay times of ~2 ms are obtained, which are similar to those in previous reports.

In previous reports, 2D material/perovskite vdWHs usually consisted of perovskites with disordered orientations. While monocrystal

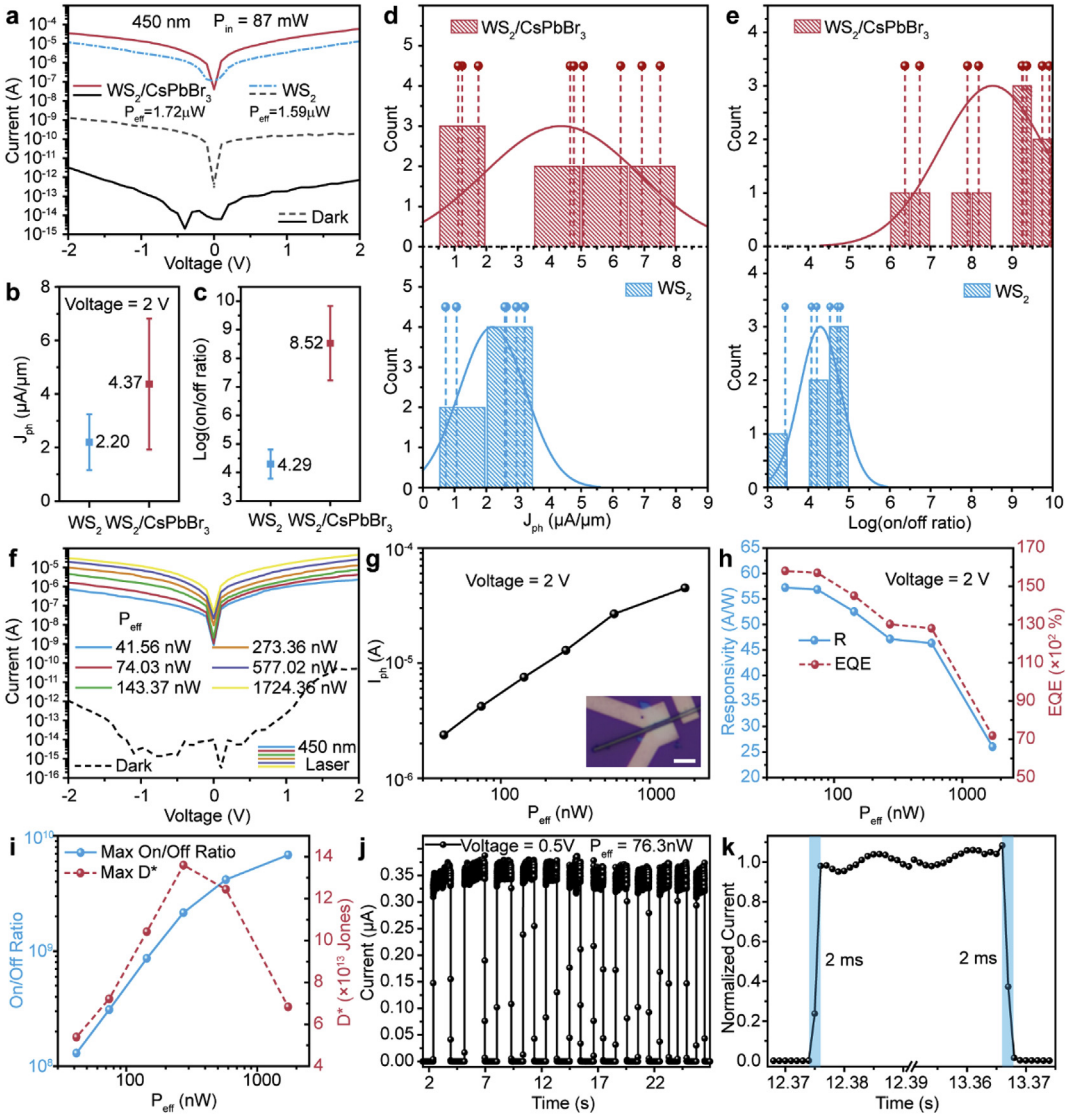

Fig. 3. Performance of $WS_2/CsPbBr_3$ vdWHs compared with pristine WS_2 and the detailed performance of the $WS_2/CsPbBr_3$ vdWH planar photodetector. (a) I-V curves of the pristine WS_2 (dashed line) and $WS_2/CsPbBr_3$ vdWH (solid line) photodetectors, respectively. (b) and (c) Statistics of J_{ph} and the maximum on/off ratio, respectively. Data are collected from six pristine WS_2 photodetectors and nine $WS_2/CsPbBr_3$ vdWH photodetectors. (d) Relevant distribution of the J_{ph} of the pristine WS_2 and $WS_2/CsPbBr_3$ vdWH photodetectors. The points with dashed lines represent experimentally obtained J_{ph} values of the devices. (e) Distribution of the maximum on/off ratio of the pristine WS_2 and $WS_2/CsPbBr_3$ vdWH photodetectors. The points with dashed lines represent experimentally obtained on/off ratio values of the devices. (f) I-V curves of the $WS_2/CsPbBr_3$ vdWH photodetector under different light intensities. (g) Corresponding light intensity dependence of I_{ph} at $V_d = 2$ V. (h) Corresponding responsivity and *EQE* of the measured photodetector under different light intensities. (i) Maximum on/off ratio and detectivity of the measured photodetectors. (j) Time-dependent photocurrent response of a device at $V_d = 0.5$ V under $P_{eff} = 76.3$ nW. (k) Partial enlargement of (j), presenting rise and decay times of both ~2 ms.

perovskite possesses uniform direction of piezo-polarization even without external applied electric field, this feature enables strain-gated and strain-sensing characteristics induced by the piezo-phototronic effect. To realize these unique characteristics, $WS_2/CsPbBr_3$ vdWH planar photodetectors are assembled on flexible PEN substrates using the same process applied on Si/SiO_2 substrates. Fig. S5 demonstrates the testing method for applying strain as well as optical images of a PEN substrate under tensile and compressive strains. Fig. 4a presents I-V curves of the flexible $WS_2/CsPbBr_3$ vdWH planar photodetector under different strains, and Fig. 4b exhibits corresponding optical micrographs of the $WS_2/CsPbBr_3$ vdWH before metal deposition, in which the diameter and length of the $CsPbBr_3$ nanowire are ~600 nm and ~115 μm, respectively. As shown in Fig. 4a, the photocurrent increases with tensile strain and decreases with compressive strain, while the effect of strain on the dark current is negligible, as presented in Fig. S6. By contrast, nearly identical I-V curves are observed for the pristine WS_2 photodetector on the PEN substrate (Fig. S7). The corresponding strain-dependent I_{ph} and responsivity are shown in Fig. 4b, and the corresponding I_{ph}/I_{ph0} and R/R_0 are presented in Fig. 4c, in which I_{ph0} and R_0 are the photocurrent and responsivity without strain, respectively. When the compressive strain increases from 0% to −0.108%, R is reduced from 0.27 to 0.06 A W^{-1}, whereas when the tensile strain increases from 0% to +0.108%, R is increased to 0.68 A W^{-1}. A value of 11.3 for I_{ph}/I_{ph0} is achieved during the strain change from −0.108% to +0.108%. Because the strain dependence of I_{ph} is approximately linear, on-chip sensing of applied strain is enabled.

The suppression of the photocurrent and responsivity for both the $WS_2/CsPbBr_3$ (Fig. 4a) and WS_2 (Fig. S7) devices on PEN are attributed to two factors, which are the transparency and inferiority of the surface SiO_2 layer of the PEN substrates. In contrast to Si/SiO_2, transparent PEN almost does not reflect incident light, which leads to limited light absorption for devices on PEN; thus, a reduced photocurrent is observed.

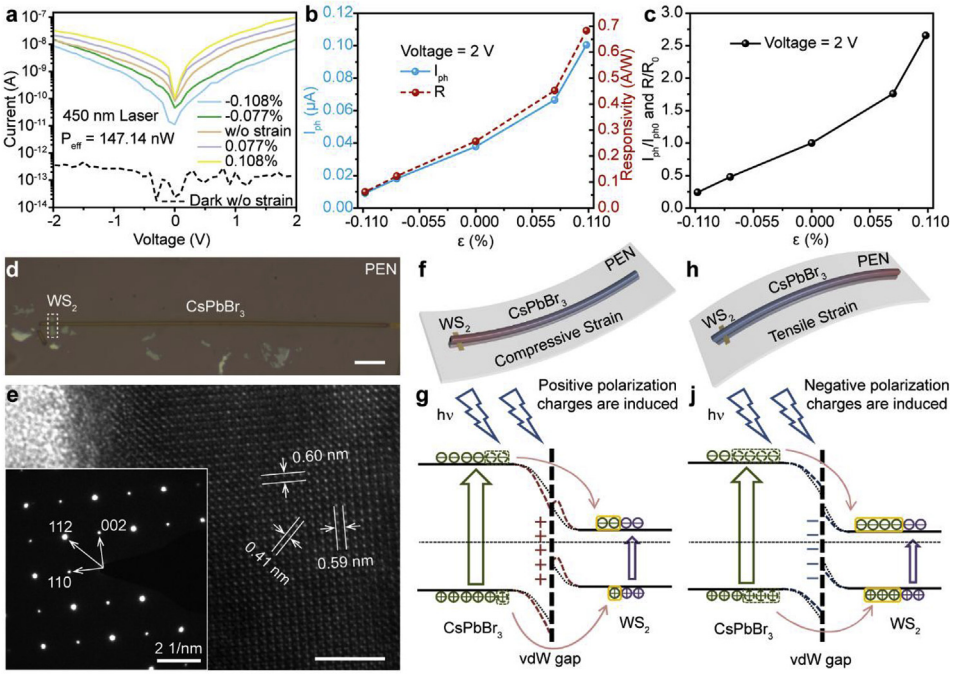

Fig. 4. Strain-gated characteristics of the WS_2/$CsPbBr_3$ vdWH planar photodetector originating from the piezo-phototronic effect. (a) I-V curves of the WS_2/$CsPbBr_3$ photodetector under different strains. (b) Corresponding strain dependence of I_{ph} and the responsivity. (c) Strain dependence of I_{ph}/I_{ph0} and R/R_0. (d) Optical micrographs of WS_2/$CsPbBr_3$ vdWHs measured in (a) before EBL and the metal deposition process. The scale bar is 10 μm. (e) HR-TEM image of the $CsPbBr_3$ nanowire; the inset presents the corresponding SAED pattern, which is indexed to an orthorhombic phase with a < 110 > zone axis. The scale bar is 5 nm. (f) Schematic illustration of the WS_2/$CsPbBr_3$ photodetector under compressive strain, in which the red part indicates a positive piezopotential, while the blue part indicates a negative piezopotential. In this case, a positive piezoelectric polarization is induced. (g) Band structure of the WS_2/$CsPbBr_3$ photodetector in (f). (h) Schematic illustration of the device under tensile strain, which induces a negative piezoelectric polarization in this case. (j) Band structure of the device in (h). Notably, the WS_2 channel is depleted; thus, the flat band part of WS_2 is included here only for convenience in depicting the excited and transferred charge carriers within WS_2, similar to in Fig. 2d.

More importantly, the SiO_2 layer is deposited on the PEN substrate by magnetron sputtering before transferring WS_2/$CsPbBr_3$ or WS_2 onto it. SiO_2 acts as an adhesion layer because the $CsPbBr_3$ nanowire cannot be directly attached to the PEN substrate. Since 2D materials are strongly sensitive to charged impurities in and the surface roughness of the substrates [28,29], the carrier mobility of WS_2 is dramatically limited by the SiO_2 layer deposited using magnetron sputtering. Novel strategies have been proposed to protect the high mobility of 2D channels from the negative impacts of a substrate. For instance, a suspended device structure [30] is appealing for completely avoiding influences from a substrate, and h-BN with an atomically smooth surface is an ideal substrate candidate for devices with high mobility [29]. However, severe limitations are imposed on device fabrication using these strategies [6,29]. Therefore, further efforts to improve the surface nature of flexible substrates are needed.

To illuminate the mechanism of the strain-gated characteristic induced by the piezo-phototronic effect, the crystal structure of the $CsPbBr_3$ nanowire is first characterized. The XRD pattern is exhibited in Fig. S9a, indicating an orthorhombic phase similar to that previously reported [23,24]. Fig. 4e and the inset present a high-resolution transmission electron microscopy (HR-TEM) image and a selected area electron diffraction (SAED) pattern of a $CsPbBr_3$ nanowire section (Fig. S9d). According to the XRD pattern and Crystallographic Information File (cif) document of orthorhombic $CsPbBr_3$, the SAED spots are indexed to (002), (112) and (110), which correspond to lattice fringes of 0.6 nm, 0.41 nm and 0.59 nm, respectively, and the zone axis is < 110 > . These results indicate the single-crystalline nature and that the crystalline growth direction is along < 110 > . Because of the low-symmetry structure of orthorhombic $CsPbBr_3$, it is proposed that when the lattice is distorted by an applied strain, piezo-polarization charges and corresponding piezopotential will be generated in $CsPbBr_3$ nanowires [20].

According to Fig. S6, in which the dark current only changes by less than 1 pA at V_d = 2 V with strain varying from −0.153% to +0.153%, the piezopotential, acting as a gate voltage, presents a relatively weak electric field modulation effect on the WS_2 channel; thus, only the piezo-phototronic effect is mainly considered. The piezo-phototronic effect is defined as the modulation of the generation, separation, diffusion and recombination of photon-induced carriers by the piezopotential [31–33]. As shown in Fig. 4f and g, when positive polarization charges are induced at the WS_2/$CsPbBr_3$ interface by strain (compressive in this case), considering the change in the work function of $CsPbBr_3$ and the constant thermal equilibrium state between WS_2 and $CsPbBr_3$, both energy bands of these two materials bend further, and only the energy band of WS_2 at the interface very slightly reversely bends due to the weak electric field modulation effect (red dashed line in Fig. 4g). The barrier for interfacial carrier transfer is strengthened, and the channel depletion overall remains. Therefore, although incident light is strongly absorbed by the perovskite, interfacial carrier transfer is difficult, and finally, the photocurrent is highly reduced. In contrast, when negative polarization charges are induced at the vdWH interface due to strain (tensile in this case), as illustrated in Fig. 4h, both energy bands of these two materials reversely bend (blue dashed line in Fig. 4j) compared with the energy bands without strain. Therefore, the barrier for interfacial carrier transfer is weakened, and thus, the interfacial carrier transfer and photocurrent are improved. In short, the strain-gated performance and strain-sensing function of the WS_2/$CsPbBr_3$ vdWH planar photodetector are induced by the piezo-phototronic effect.

4. Conclusion

In conclusion, 2D-WS_2/1D-$CsPbBr_3$ vdWH planar photodetectors are assembled and characterized for the first time. Efficient charge carrier transfer from $CsPbBr_3$ to WS_2 is verified by the reduction in the PL intensity compared to pristine $CsPbBr_3$. Light-induced carrier transfer to WS_2 and depletion of the WS_2 channel enable simultaneous increase of the photocurrent and decrease of the dark current, as demonstrated by the I-V curves and ultrahigh on/off ratio of the WS_2/$CsPbBr_3$ vdWH planar photodetector. In addition to an on/off ratio of up to $10^{9.83}$, the highest R, D^* and EQE are 57.2 A W^{-1}, 1.36×10^{14} Jones and 157, respectively. The I-T curves show fast rise and decay times of ~2 ms. Moreover, owing to the high crystal quality of mechanically exfoliated 2D WS_2, the WS_2/$CsPbBr_3$ photodetector can still present incredible performance even at a V_d of 0.5 V. The piezoelectric property of monocrystalline $CsPbBr_3$ nanowires endow WS_2/$CsPbBr_3$ photodetectors with strain-gated characteristics and a strain-sensing function induced by the piezo-phototronic effect. Modulation of I_{ph} and

R by a factor of 11.3 is achieved, and the linear strain dependence of I_{ph} enables on-chip strain sensing for WS_2/$CsPbBr_3$ devices. This work illustrates a new device design for photodetectors with high performance, low energy consumption and multifunction integration toward emerging technologies.

Acknowledgements

The authors thank the support of national key R & D project from Minister of Science and Technology, China (2016YFA0202703), National Natural Science Foundation of China (No. 51622205, 61675027, 51432005, 61505010 and 51502018), Beijing City Committee of science and technology (Z171100002017019 and Z181100004418004), Beijing Natural Science Foundation (4181004, 4182080, 4184110 and 2184131), and the University of Chinese Academy of Sciences.

Appendix A. Supplementary data

Supplementary data to this article can be found online at https://doi.org/10.1016/j.nanoen.2019.104001.

References

Uncategorized References

[1] Q.H. Wang, K. Kalantar-Zadeh, A. Kis, J.N. Coleman, M.S. Strano, Electronics and optoelectronics of two-dimensional transition metal dichalcogenides, Nat. Nanotechnol. 7 (2012) 699.
[2] G. Konstantatos, M. Badioli, L. Gaudreau, J. Osmond, M. Bernechea, F.P.G. de Arquer, F. Gatti, F.H.L. Koppens, Hybrid graphene–quantum dot phototransistors with ultrahigh gain, Nat. Nanotechnol. 7 (2012) 363.
[3] P. Lin, L. Zhu, D. Li, L. Xu, C. Pan, Z. Wang, Piezo-phototronic effect for enhanced flexible MoS_2/WSe_2 van der Waals photodiodes, Adv. Funct. Mater. 28 (2018) 1802849.
[4] Q. Fang, Q. Shang, L. Zhao, R. Wang, Z. Zhang, P. Yang, X. Sui, X. Qiu, X. Liu, Q. Zhang, Y. Zhang, Ultrafast charge transfer in perovskite nanowire/2D transition metal dichalcogenide heterostructures, J. Phys. Chem. Lett. (2018) 1655.
[5] M. Patel, J. Kim, Y.K. Kim, Growth of large-area SnS films with oriented 2D SnS layers for energy-efficient broadband optoelectronics, Adv. Funct. Mater. 28 (2018).
[6] F. Pizzocchero, L. Gammelgaard, B.S. Jessen, J.M. Caridad, L. Wang, J. Hone, P. Bøggild, T.J. Booth, The hot pick-up technique for batch assembly of van der Waals heterostructures, Nat. Commun. 7 (2016) 11894.
[7] M. Kumar, H.-S. Kim, J. Kim, A highly transparent artificial photonic nociceptor, Adv. Mater. 31 (2019).
[8] M. Patel, D.-K. Ban, A. Ray, J. Kim, Transparent all-oxide photovoltaics and broadband high-speed energy-efficient optoelectronics, Sol. Energy Mater. Sol. Cells 194 (2019) 148.
[9] F. Li, J. Lu, Q. Zhang, D. Peng, Z. Yang, Q. Xu, C. Pan, A. Pan, T. Li, R. Wang, Controlled fabrication, lasing behavior and excitonic recombination dynamics in single crystal $CH_3NH_3PbBr_3$ perovskite cuboids, Sci. Bull. 64 (2019) 698–704.
[10] M. Gao, Halide perovskite nanocrystals can also stand luminescent in water, Sci. Bull. 63 (2018) 1241.
[11] Z. Yang, Q. Xu, X. Wang, J. Lu, H. Wang, F. Li, L. Zhang, G. Hu, C. Pan, Large and ultrastable All-inorganic $CsPbBr_3$ monocrystalline films: low-temperature growth and application for high-performance photodetectors, Adv. Mater. 30 (2018) 1802110.
[12] D.-H. Kang, S.R. Pae, J. Shim, G. Yoo, J. Jeon, J.W. Leem, J.S. Yu, S. Lee, B. Shin, J.-H. Park, An ultrahigh-performance photodetector based on a perovskite-transition-metal-dichalcogenide hybrid structure, Adv. Mater. 28 (2016) 7799.
[13] Y. Lee, J. Kwon, E. Hwang, C.-H. Ra, W.J. Yoo, J.-H. Ahn, J.H. Park, J.H. Cho, High-performance perovskite-graphene hybrid photodetector, Adv. Mater. 27 (2015) 41.
[14] Y. Wang, R. Fullon, M. Acerce, C.E. Petoukhoff, J. Yang, C. Chen, S. Du, S.K. Lai, S.P. Lau, D. Voiry, D. O'Carroll, G. Gupta, A.D. Mohite, S. Zhang, H. Zhou, M. Chhowalla, Solution-processed MoS_2/organolead trihalide perovskite photodetectors, Adv. Mater. 29 (2017) 1603995.
[15] C. Ma, Y. Shi, W. Hu, M.-H. Chiu, Z. Liu, A. Bera, F. Li, H. Wang, L.-J. Li, T. Wu, Heterostructured WS_2/$CH_3NH_3PbI_3$ photoconductors with suppressed dark current and enhanced photodetectivity, Adv. Mater. 28 (2016) 3683.
[16] H. Chengxue, L. Xuhai, W. Ziming, S. Xiufeng, Z. Haibo, High-performance low--voltage-driven phototransistors through $CsPbBr_3$–2d crystal van der Waals heterojunctions, Adv. Opt. Mater., 0, 1800152.
[17] H. Wu, Z. Kang, Z. Zhang, Z. Zhang, H. Si, Q. Liao, S. Zhang, J. Wu, X. Zhang, Y. Zhang, Interfacial charge behavior modulation in perovskite quantum dot-monolayer MoS_2 0D-2D mixed-dimensional van der Waals heterostructures, Adv. Funct. Mater. 28 (2018).
[18] J. Lu, A. Carvalho, H. Liu, S.X. Lim, A.H. Castro Neto, C.H. Sow, Hybrid bilayer WSe_2-$CH_3NH_3PbI_3$ organolead halide perovskite as a high-performance photodetector, Angew. Chem. Int. Ed. 55 (2016) 11945.
[19] M. Spina, M. Lehmann, B. Náfrádi, L. Bernard, E. Bonvin, R. Gaál, A. Magrez, L. Forró, E. Horváth, Microengineered $CH_3NH_3PbI_3$ nanowire/graphene phototransistor for low-intensity light detection at room temperature, Small 11 (2015) 4824.
[20] Z. Yang, J. Lu, M. ZhuGe, Y. Cheng, J. Hu, F. Li, S. Qiao, Y. Zhang, G. Hu, Q. Yang, D. Peng, K. Liu, C. Pan, Controllable growth of aligned monocrystalline $CsPbBr_3$ microwire arrays for piezoelectric-induced dynamic modulation of single-mode lasing, Adv. Mater. 0 (2019) e1900647.
[21] W. Wu, Z.L. Wang, Piezotronics and piezo-phototronics for adaptive electronics and optoelectronics, Nat. Rev. Mater. 1 (2016).
[22] J. Feng, X. Yan, Y. Liu, H. Gao, Y. Wu, B. Su, L. Jiang, Crystallographically aligned perovskite structures for high-performance polarization-sensitive photodetectors, Adv. Mater. 29 (2017) 1605993.
[23] D. Zhang, S.W. Eaton, Y. Yu, L. Dou, P. Yang, Solution-phase synthesis of cesium lead halide perovskite nanowires, J. Am. Chem. Soc. 137 (2015) 9230.
[24] Y. Fu, H. Zhu, C.C. Stoumpos, Q. Ding, J. Wang, M.G. Kanatzidis, X. Zhu, S. Jin, Broad wavelength tunable robust lasing from single-crystal nanowires of cesium lead halide perovskites (CsPbX3, X = Cl, Br, I), ACS Nano 10 (2016) 7963.
[25] N. Perea-Lopez, A.L. Elias, A. Berkdemir, A. Castro-Beltran, H.R. Gutierrez, S. Feng, R. Lv, T. Hayashi, F. Lopez-Urias, S. Ghosh, B. Muchharla, S. Talapatra, H. Terrones, M. Terrones, Photosensor device based on few-layered WS_2 films, Adv. Funct. Mater. 23 (2013) 5511.
[26] A. Berkdemir, H.R. Gutiérrez, A.R. Botello-Méndez, N. Perea-López, A.L. Elías, C.-I. Chia, B. Wang, V.H. Crespi, F. López-Urías, J.-C. Charlier, H. Terrones, M. Terrones, Identification of individual and few layers of WS_2 using Raman Spectroscopy, Sci. Rep. 3 (2013) 1755.
[27] J. Wang, H. Fang, X. Wang, X. Chen, W. Lu, W. Hu, Recent progress on localized field enhanced two-dimensional material photodetectors from ultraviolet-visible to infrared, Small 13 (2017).
[28] X. Cui, G.-H. Lee, Y.D. Kim, G. Arefe, P.Y. Huang, C.-H. Lee, D.A. Chenet, X. Zhang, L. Wang, F. Ye, F. Pizzocchero, B.S. Jessen, K. Watanabe, T. Taniguchi, D.A. Muller, T. Low, P. Kim, J. Hone, Multi-terminal transport measurements of MoS2 using a van der Waals heterostructure device platform, Nat. Nanotechnol. 10 (2015) 534.
[29] C.R. Dean, A.F. Young, I. Meric, C. Lee, L. Wang, S. Sorgenfrei, K. Watanabe, T. Taniguchi, P. Kim, K.L. Shepard, J. Hone, Boron nitride substrates for high-quality graphene electronics, Nat. Nanotechnol. 5 (2010) 722.
[30] X. Du, I. Skachko, A. Barker, E.Y. Andrei, Approaching ballistic transport in suspended graphene, Nat. Nanotechnol. 3 (2008) 491.
[31] C. Pan, L. Dong, G. Zhu, S. Niu, R. Yu, Q. Yang, Y. Liu, Z.L. Wang, High-resolution electroluminescent imaging of pressure distribution using a piezoelectric nanowire LED array, Nat. Photonics 7 (2013) 752.
[32] S. Qiao, J. Liu, G. Fu, K. Ren, Z. Li, S. Wang, C. Pan, ZnO nanowire based CIGS solar cell and its efficiency enhancement by the piezo-phototronic effect, Nano Energy 49 (2018) 508.
[33] X. Wang, D. Peng, B. Huang, C. Pan, Z.L. Wang, Piezophotonic effect based on mechanoluminescent materials for advanced flexible optoelectronic applications, Nano Energy 55 (2019) 389.

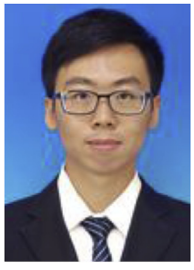

Qian Xu received his B.S. degree in Applied Chemistry from Beijing University of Chemical Technology, China in 2012 and Master degree in Chemical Engineering from Tianjin University, China in 2015. He is pursuing his doctor degree under the supervision of Prof. Caofeng Pan at Beijing Institute of Nanoenergy and Nanosystems, CAS. His main research interests focus on the fields of novel electronic and optoelectronic micro/nano-devices.

Zheng Yang received his B.S. degree in Materials Science and Engineering from Tsinghua University, China in 2010 and Master degree in Materials Physics and Chemistry from The Xinjing Technical Institute of Physics & Chemistry, CAS in 2016. He is currently studying in Nano science and technology as a doctor at Beijing Institute of Nanoenergy and Nanosystems, CAS. His main research interests focus on the fields of perovskite optoelectronic devices and piezotronic/piezophototronic devices.

Dr. Dengfeng Peng was born in Hubei, China. He received his BS degree (2006) in Physics from Xinjiang University and Ph.D. degree (2013) in Materials Science and Engineering from Tongji University. He spent one year as a joint PhD student at AIST in Japan. He carried out post-doctoral research work at City University of Hong Kong in (2013), BINN Chinese Academy of Sciences (2015), and The Hong Kong Polytechnic University (2016). He joined the Shenzhen University in 2017. His research interests include the synthesis and mechanistic investigation of functional luminescent materials for applications in optoelectronic and advanced energy devices.

Dr. Jianguo Xi received his B. S. Degree (2010) in Materials Science and Engineering from Taiyuan University of Science and Technoloygy, and then graduated from China University of Geosciences as a Ph. D. (2015). He then joined Materials Engineering of Auburn University as a postdoctoral fellow. He is currently a joint postdoctor of Dr. Wenjie Mai's group at Jinan University and Dr. Canfeng Pan's group at Beijing Institute of Nanoenergy and Nanosystem, China Academy of Sciences since 2019. His research interests focus on the fields of 2D Van Der Waals heterostructures and the application in the piezoelectric and piezophototronic devices.

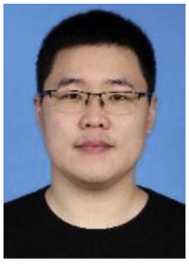

Dr. Pei Lin received his Ph.D. degree in Materials Science and Engineering (MSE) from University of Science and Technology Beijing in 2016. He then joined the group of Prof. Zhonglin Wang at Beijing Institute of Nanoenergy and Nanosystems, CAS as a postdoctoral fellow. His research interests focus on the fields of piezotronics/piezo-phototronics for application in smart human-machine interfacing and self-powered systems.

Yang Cheng received his B.S. degree from Nankai University and then he joined the Ultrafast Nano-optics group of Prof. Kaihui Liu in 2016. His research interests are characterizing light-matter interactions and physical properties of low-dimensional nanomaterials and material interfaces through optical method.

Prof. Kaihui Liu is currently a Professor of Physics, Peking University. He got his PhD degree from Institute of Physics, CAS of China, under Prof. Enge Wang in 2009. After that he worked as a postdoctoral fellow at Department of Physics, UC Berkeley, in Prof. Feng Wang's group. In 2014, he joined Peking University as the National Thousand Youth Talents Plan Professor of China. His main research interests are the novel physical phenomena and controllable growth in nanoscale structures, especially meter-sized 2D single crystals.

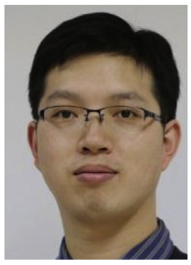

Prof. Caofeng Pan received his B.S. degree (2005) and his Ph.D. (2010) in Materials Science and Engineering from Tsinghua University, China. He then joined the Georgia Institute of Technology as a postdoctoral fellow. He is currently a professor and a group leader at Beijing Institute of Nanoenergy and Nanosystems, Chinese Academy of Sciences since 2013. His main research interests focus on the fields of piezotronics/piezo-phototronics for fabricating new electronic and optoelectronic devices, and self-powered nanosystems. Details can be found at http://www.piezotronics.cn.